



# Hybrid High-order Eulerian-Lagrangian methods for simulations of particle-laden flow with shocks

Jean-Piero Suarez

June 2012

Publication Number: CSRCR2012-01

Computational Science &  
Engineering Faculty and Students  
Research Articles

Database Powered by the  
Computational Science Research Center  
Computing Group & Visualization Lab

## COMPUTATIONAL SCIENCE & ENGINEERING



**SAN DIEGO STATE  
UNIVERSITY**

Computational Science Research Center  
College of Sciences  
5500 Campanile Drive  
San Diego, CA 92182-1245  
(619) 594-3430



Hybrid High-order Eulerian-Lagrangian methods for  
simulations of particle-laden flow with shocks

Jean-Piero Suarez \*

*Computational Science Research Center,  
San Diego State University, San Diego*

Gustaaf B. Jacobs †

*Department of Aerospace Engineering & Engineering Mechanics,  
San Diego State University, San Diego*

June 5, 2012

---

\*E-Mail: [jsuarez@sciences.sdsu.edu](mailto:jsuarez@sciences.sdsu.edu)

†E-Mail: [gjacobs@mail.sdsu.edu](mailto:gjacobs@mail.sdsu.edu)

## Abstract

The development of a Hybrid high order Eulerian-Lagrangian algorithm to simulate shock wave interactions with particles is discussed. The Hybrid high order WENO/central finite difference scheme is assessed in three-dimensional simulations, as well as the effective use of the high order polynomials and regularization techniques in the approximation to the singular source term in the advection equation. The mathematical model is based on a coupled system, consisting of a non-linear hyperbolic conservation laws with a source term that accounts the influence of the particles on the flow and kinematic equations, which govern the fluid flow and particle motion, respectively. The continuum conservation equations solve the carrier flow with a Hybrid scheme that uses the weighted essentially non-oscillatory (WENO) method for shock capturing, and a more computationally efficient high order scheme, including a central finite difference or spectral methods in regions where the solution is smooth. Numerical experiments illustrate the accuracy and efficiency of the Hybrid code compared with the pure WENO. Initial efforts have been made towards the development of a Hybrid WENO-spectral particle-source-in-cell (PSIC) algorithm. Specifically, a new regularization of the singular source term through polynomial approximations that couples particles and fluid have shown regularize discontinuities while converging at higher error away from discontinuity.

## 1 Introduction

Computational simulation of particle dispersion in a shocked flow is of central importance in many applications of sciences and engineering. Often, shocks will interact with solid or liquid particles and the prediction of the particle position after contact with the shock wave can be very useful in industrial design. Simulations of dust explosions in coal mines, solid propellant combustion in

rocket engines and mixtures of gases heavily laden with particles in powder metallurgy are notable examples.

The full analysis of fluid particle interaction involves computation of the complete flow over each particle, the tracking of individual solid or liquid complex particle boundaries along their paths, and the tracking of shock waves in the moving frame. These individual computational components are difficult to resolve and currently barely within reach, even with the latest advances of computational technologies. The combined interaction between flows with shocks and particles has an immense complexity, scale range and size, that can currently potentially be analyzed only in highly idealized situation with a few particles. In that sense, is desirable the use of simplified models that allows computational simulation with a large number of particles, in order to approach realistic situations in science or engineering applications.

The particle-source-in-cell (PSIC) method facilitates affordable computations of real geometries, while accurately representing individual particle dynamics. It is a particle-mesh type algorithm where the continuum model is approximated on a static mesh, while the particle dynamics are modeled as singular points and are traced along their path in a Lagrangian frame. The particles are assumed to have a single point contribution and are carried by the carrier flow that is governed by a continuum equation. The influence of the particles on the carrier flow is modeled through point sources and appears as source terms in the continuum equations. The point modeling permits the simulation of a large number of particles and provides sufficient resolution and accuracy to model the particle-laden flows.

The Mathematical model is formulated by the coupled system:

$$\left\{ \begin{array}{l} \frac{\partial \mathbf{Q}}{\partial t}(\mathbf{x}, t) + \nabla \cdot \mathbf{F}(\mathbf{Q}) = \underbrace{\sum \mathbf{K}(\mathbf{x}_p, \mathbf{x}) \mathbf{F}_p}_{\mathbf{S}(\mathbf{x}_p, \mathbf{x})}, \\ \frac{d\mathbf{x}_p}{dt} = \mathbf{v}_p, \\ m_p \frac{d\mathbf{v}_p}{dt} = \mathbf{F}_p, \end{array} \right. \quad (1)$$

where the last two equations govern the position  $\mathbf{x}_p$  and acceleration  $\frac{d\mathbf{v}_p}{dt}$  of a particle of mass  $m_p$  through a kinematic equation and the Newton's second law forced by the drag  $\mathbf{F}_p$  on the particle, respectively. The first equation comprise the continuum model, which is represented by non-linear hyperbolic conservation laws, where  $\mathbf{Q}$  and  $\mathbf{F}$  are vectors with conserved quantities and the fluxes, and  $\mathbf{S}$ , is the source term that accounts for the effect of the particles on the flow by the weighing function  $\mathbf{K}(\mathbf{x}_p, \mathbf{x})$ .

The computational solution of (1) exhibit both fine scale and structures of the physical phenomena require and shocks. The use of very accurate methods with shock capturing capability, suitable for implementation in modern parallel supercomputers and graphics processing units is desired.

The high order weighted essentially non-oscillatory (WENO) method [4] has proven to be very effective capturing shocks in the numerical solution of hyperbolic conservations laws [6]. However, the implementation of this method is computationally costly and unnecessary in physical regions where the solution is in a stable manner sufficiently smooth. Central finite difference is more efficient, but can not capture shocks. This work has focused on the development of a high order PSIC scheme, based on WENO for shock capturing and a different and more computationally efficient high order scheme in smooth regions. We have focused on the assessment of a 3D Hybrid flow solver and the higher order coupling between the Hybrid and the particle solver. To couple particles to fluid, a smooth higher order weighting function  $\mathbf{K}$  is advisable to evaluate the source

term, in order to ensure a low noise and accurate coupling of the particles to the flow. A lack of smoothness of the particle shape results in Gibbs type phenomena that affect accuracy and introduce noise in the source term,  $\mathcal{S}$ . Non-smooth shapes also enhance instability [3].

We discuss an extension of the work presented in [14], where a high order Hybrid scheme that switches between WENO high order central finite difference scheme (CFD) based on a higher order multi-resolution (MR) analysis [12], was developed in two dimensions. We have extended this Hybrid scheme to three-dimensions and we assess the performance of the Hybrid scheme in terms of speed and accuracy in parallel computations of a three-dimensional circular sonic jet in supersonic cross flow in [1], following the benchmark experiment performed in [32]. We investigate the performance of the Hybrid scheme in terms of accuracy for a long time integration and in terms of the efficiency measured with CPU timing running on a parallel machine. The Hybrid scheme is shown to be up to 40% more computationally efficient than the pure WENO scheme for the injector benchmark. The results computed with various orders of the Hybrid scheme and different grid resolutions are in good agreement with those computed with a pure WENO scheme.

The next step is the development of a multi-domain spectral-WENO method to solve the coupled system (1). In this version, instead of CFD, we will use spectral methods [2] to deal with the smooth parts of the solution, which are non-dispersive, non-dissipative and exhibit exponential convergence rate for smooth problems. In addition, subdomain adaptivity based on MR analysis is used to maintain shocks inside WENO subdomains and smooth parts in spectral ones

When the spectral method is used in the spatial discretization, the evaluation of the source term in the coupled model (1) can induce artificial Gibbs oscillations, affecting considerably the accuracy in the numerical solution. An extensive study of this phenomenon has been presented in [7, 8] for

the one dimensional linear advection equation with a non-stationary singular source term given by  $\delta$ -function, where the WENO scheme and the spectral Chebyshev collocation method with Gauss-Lobatto nodes were used for spatial discretization and, the direct projection (DP) method and Gaussian (G) function to approximate the source term.

The numerical solution of the one dimensional advection equation plays an important role in our problem mainly because of any algorithm developed for its numerical solution can be generalized to the case of non-linear conservation laws [5]. We have developed approximations for the non-stationary singular source term in order to obtain an accurate and stable numerical solution. We develop of regularization techniques and high order polynomials with compact support for which, the accuracy in the approximation to the source term depends on the smoothness and vanishing moments of the respective function. Numerical results in the solution of one dimensional advection equation, shows the effectiveness of this techniques in terms of accuracy, when the spectral Chebyshev collocation method with Gauss-Lobatto nodes is used.

There are two main contributions in this work to distinguish: the three dimensional WENO/central finite difference scheme implemented to solve conservation laws and the solution of the one dimensional advection equation with a singular source term, which are described in sections 2 and 3, respectively.

In section 2, a brief introduction to the Hybrid scheme and its algorithm is given. The central finite difference scheme, WENO finite difference scheme and the Multi-Resolution analysis are briefly described in sections 2.1, 2.2 and 2.3 respectively. Section 2.5 discusses the application of the Hybrid scheme to the three dimensional circular sonic jet injection into a supersonic cross flow. The computational results using both the pure WENO scheme and Hybrid scheme are presented

and the performance of the Hybrid scheme is discussed.

In section 3 is presented the singular advection equation. The spectral Chebyshev collocation method applied to this problem and the methods to approximate the  $\delta$ -function are described in sections 3.1 and 3.2, respectively. Section 3.3 contains numerical results and discussion in the solution of the advection equation with the different approximations to the singular source term. Finally, conclusions and remarks on the implementation of the Hybrid scheme and the solution of the singular advection equation are given in sections 2.6 and 3.4, respectively.

## 2 Hybrid Central-WENO finite difference scheme

A hybrid scheme that hybridizes the high order non-dissipative central finite difference scheme (CFD) and an improved high order weighted essentially non-oscillatory scheme (WENO-Z) presented in [14] is presented for solution of the three-dimensional Euler equations.

The well-known equations comprise a system of non-linear hyperbolic conservation laws that can be written compactly as

$$\frac{\partial \mathbf{Q}}{\partial t} + \nabla \cdot \mathbf{F}(\mathbf{Q}) = 0. \quad (2)$$

The system is discretized on a Cartesian uniformly spaced mesh in a three dimensional rectangular physical domain. The central finite difference scheme is employed in regions where the flow solution is smooth. The WENO-Z finite difference scheme is employed otherwise to capture discontinuities in the flow solution such as shocks and contact discontinuities whose formation is closely related to the nonlinear nature of (2). To determine the smoothness of solution in the computational domain and to maintain the high order (resolution) nature of the Hybrid scheme, the high order

multi-resolution analysis (MR) by Harten [12] is employed to switch between CFD and WENO schemes. The temporal and spatial adaptation of the two high order (resolution) schemes allows one to take advantages of the fast non-dissipative CFD solver for an accurate and efficient long time simulations while sharp gradients and shocks are captured in an essentially non-oscillatory manner by the WENO scheme.

We briefly review the three individual high order (resolution) components of the Hybrid method, including the CFD, WENO-Z, and MR schemes followed by a summary of the Hybrid algorithm. For a more detailed description, we refer to [14]. We present the schemes in one space dimension. Following a method of lines, the one-dimensional method extends naturally to multi-dimensions in Cartesian coordinates.

## 2.1 Central Finite Difference Scheme (CFD)

A central finite difference scheme (CFD) of order  $n$  approximates the derivative of a function at a grid point  $x_i$  on a Cartesian uniformly spaced mesh as follows

$$\frac{d}{dx}f(x_i) = \frac{1}{\Delta x} \sum_{j=-n}^n w_j f_{i+j}, \quad (3)$$

where  $w_j$  are the Lagrangian weights of the first derivative [23].

Whereas the CFD scheme is non-dissipative, it does suffer from numerical dispersive errors that introduce artificial high-frequency waves in the solution. To prevent these high-frequency oscillations from causing numerical instabilities, a high order smoothing is required to remove them. For a given function  $f(x)$ , discretized on a uniformly spaced grid, a filtered function of order  $n$ ,  $\hat{f}(x)$ ,

at the grid point  $x_i$  can be expressed as

$$\hat{f}_i = \sum_{j=-n}^n \alpha_j f_{i+j}, \quad (4)$$

where  $\alpha_j$  are the filtering weights which satisfy the symmetry property  $\alpha_{-j} = \alpha_j$ . The coefficients  $\alpha_j$  are chosen in such a way that the first  $n$  moments of the filtered function match exactly the first  $n$  monomials  $\{1, x, \dots, x^n\}$  ensuring that the approximation order of the filtered function is kept high. In addition to that, the  $\alpha_j$  are also required to satisfy the condition  $\sum_{j=-n}^n \alpha_j (-1)^j = 0$  so that oscillations at high wavenumbers are attenuated to zero. Some of these high order filtering weights  $\alpha_j$  can be found in [24].

## 2.2 Weighted Essentially Non-Oscillatory Scheme

WENO captures discontinuities in the flow solution in an essentially non-oscillatory manner and resolves the high frequency waves accurately. We consider the characteristics based weighted essentially non-oscillatory conservative finite difference scheme (WENO-Z) for the solution of the system of hyperbolic conservation laws of order,  $(2r - 1)$ . We present the explicit formula for a fifth ( $r = 3$ ) order scheme. Extension to higher order ( $r > 3$ ) WENO scheme is straightforward as explained in [18].

Consider a uniform spaced grid defined by the points  $x_i = i\Delta x, i = 0, \dots, N$ , which are called cell centers, with cell boundaries given by  $x_{i+\frac{1}{2}} = x_i + \frac{\Delta x}{2}$ , where  $\Delta x$  is the uniform grid spacing (see Fig. 1). The semi-discretized form of (2) is transformed into the system of ordinary differential equations and solved by the method of lines

$$\frac{dQ_i(t)}{dt} = - \left. \frac{\partial f}{\partial x} \right|_{x=x_i}, \quad i = 0, \dots, N, \quad (5)$$

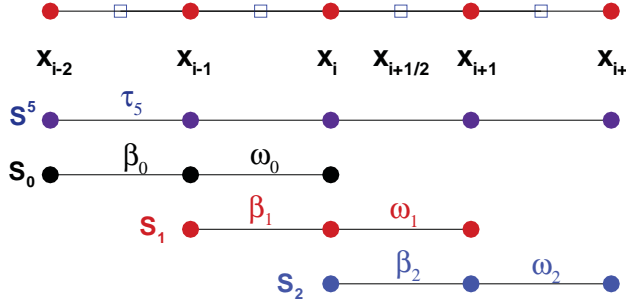


Figure 1: The computational uniformly spaced grid  $x_i$  and the 5-points stencil  $S^5$ , composed of three 3-points substencils  $S_0, S_1, S_2$ , used for the fifth-order WENO reconstruction step.

where  $Q_i(t)$  is a numerical approximation to the cell-averaged value  $Q(x_i, t)$ .

To form the flux differences across the uniformly spaced cells and to obtain high-order numerical fluxes consistent with the hyperbolic conservation laws, a conservative finite-difference formulation is required at the cell boundaries. We implicitly define the numerical flux function  $h(x)$  as

$$f(x) = \frac{1}{\Delta x} \int_{x-\frac{\Delta x}{2}}^{x+\frac{\Delta x}{2}} h(\xi) d\xi, \quad (6)$$

such that the spatial derivative in (5) is approximated by a conservative finite difference formula at the cell boundaries  $x_{i\pm\frac{1}{2}}$ ,

$$\frac{du_i(t)}{dt} = -\frac{1}{\Delta x} \left( h_{i+\frac{1}{2}} - h_{i-\frac{1}{2}} \right), \quad (7)$$

where  $h_{i\pm\frac{1}{2}} = h(x_{i\pm\frac{1}{2}})$ . High order polynomial interpolations to  $h_{i\pm\frac{1}{2}}$  are computed using known cell-averaged values  $f_j = f(x_j), j = i - r + 1, \dots, i + r - 1$ .

The  $(2r - 1)$  order WENO scheme uses a  $(2r - 1)$ -points global stencil, which is subdivided into  $r$  substencils  $\{S_0, S_1, \dots, S_{r-1}\}$  with each substencil containing  $r$  grid points and a global stencils

$S^{2r-1} = \bigcup_{i=0}^{r-1} S_i$ . For  $r = 3$ , the 5-points global stencil, hereafter named  $S^5$ , is subdivided into three 3-points substencils  $\{S_0, S_1, S_2\}$ .

The  $(2r-1)$  degree polynomial approximation  $\hat{f}_{i\pm\frac{1}{2}} = h_{i\pm\frac{1}{2}} + O(\Delta x^{2r-1})$  is built through the convex combination of the lower  $r$  degree polynomial  $\hat{f}^k(x)$  in substencils  $S_k$  at the cell boundary  $x_{i\pm\frac{1}{2}}$ :

$$\hat{f}_{i\pm\frac{1}{2}} = \sum_{k=0}^{r-1} \omega_k^\pm \hat{f}^k(x_{i\pm\frac{1}{2}}), \quad (8)$$

where

$$\hat{f}^k(x_{i+\frac{1}{2}}) = \sum_{j=0}^{r-1} c_{kj} f_{i-k+j}, \quad i = 0, \dots, N. \quad (9)$$

The  $c_{kj}$  are Lagrangian interpolation coefficients [11] and  $\omega_k$  are normalized nonlinear weights (weights), which will be described below.

The regularity of the  $(r-1)$  degree interpolation polynomial approximation  $\hat{f}^k(x)$  at the substencil  $S_k$  is measured by the lower order local smoothness indicators  $\beta_k$ , which are given by

$$\beta_k = \sum_{l=1}^{r-1} \Delta x^{2l-1} \int_{x_{i-\frac{1}{2}}}^{x_{i+\frac{1}{2}}} \left( \frac{d^l}{dx^l} \hat{f}^k(x) \right)^2 dx, \quad k = 0, \dots, r-1. \quad (10)$$

For  $r = 3$ , the  $\beta_k$  in terms of the cell averaged values  $f_i = f(x_i)$  are given explicitly by

$$\beta_0 = \frac{13}{12} (f_{i-2} - 2f_{i-1} + f_i)^2 + \frac{1}{4} (f_{i-2} - 4f_{i-1} + 3f_i)^2, \quad (11)$$

$$\beta_1 = \frac{13}{12} (f_{i-1} - 2f_i + f_{i+1})^2 + \frac{1}{4} (f_{i-1} - f_{i+1})^2, \quad (12)$$

$$\beta_2 = \frac{13}{12} (f_i - 2f_{i+1} + f_{i+2})^2 + \frac{1}{4} (3f_i - 4f_{i+1} + f_{i+2})^2. \quad (13)$$

The WENO-Z scheme makes use of the higher order information obtained from a global optimal order smoothness indicator  $\tau_{2r-1}$  which is built as a linear combination of  $\beta_k$ , that is,

$$\tau_{2r-1} = \sum_{k=0}^{r-1} c_k \beta_k, \quad (14)$$

where  $c_k$  are given constants [17, 18]. For  $r = 3$ , one has  $\tau_5 = |\beta_0 - \beta_2|$ , which is of order  $O(\Delta x^5)$ .

The normalized and un-normalized nonlinear weights  $\omega_k^Z$  and  $\alpha_k^Z$ , respectively, are defined as

$$\omega_k^Z = \frac{\alpha_k^Z}{\sum_{l=0}^{r-1} \alpha_l^Z}, \quad \alpha_k^Z = \frac{d_k}{\beta_k^Z} = d_k \left( 1 + \left( \frac{\tau_{2r-1}}{\beta_k + \epsilon} \right)^p \right), \quad k = 0, \dots, r-1, \quad (15)$$

The parameter  $\epsilon$  (typically  $10^{-12}$ ) is used to avoid the division by zero in the denominator and power parameter  $p$  (typically  $p = 2$ ) is chosen to increase the difference of scales of distinct weights at non-smooth parts of the solution. The coefficients  $\{d_0, d_1, \dots, d_{r-1}\}$  are called the ideal weights since they generate the  $(2r - 1)$  order central upwind scheme when the solution is smooth. For  $r = 3$ , the ideal weights are  $\{d_0 = \frac{3}{10}, d_1 = \frac{3}{5}, d_2 = \frac{1}{10}\}$ .

Following [17, 18], the hyperbolicity of the Euler equations admits a complete set of right and left eigenvectors for the Jacobian of the system. The approximated eigenvalues and eigenvectors are obtained via the Roe averaged Jacobian. The first order global Lax-Friedrichs flux is used as the low order building block for the high order reconstruction step of the WENO scheme. After projecting the positive and negative fluxes on the characteristic fields via the left eigenvectors, the high order WENO reconstruction step is applied to obtain the high order approximation at the cell boundaries using the surrounding cell-centered values, which are then projected back into the physical space via the right eigenvectors and added together to form a high order numerical flux at the cell-interfaces. The conservative difference of the reconstructed high order fluxes can then be computed for inviscid flux.

The resulting system of ordinary differentiation equations ODE (3) and (7) remain after the spatial discretization are advanced in time via the third order TVD Runge-Kutta scheme [17]. The CFL condition is set to be  $\text{CFL} = 0.45$  in the numerical experiments performed in this study.

### 2.3 Multi-Resolution Analysis (MR)

The Multi-Resolution analysis (MR) measures the smoothness of the solution at each grid point at a given time and quantifies the smoothness through a MR coefficient. Since the WENO-Z and

CFD schemes are both high order schemes, the measure of the smoothness of the solution must also be of high order in order to differentiate a high frequency wave from a high gradient/shock so that the appropriate numerical spatial scheme (CFD for high-frequency wave or WENO-Z for shocks) can be applied at a given spatial location and at a given time. To do so, the high order multi-level Multi-Resolution (MR) algorithm by Harten [12] is employed to detect the smooth and rough parts of the solution.

Given an initial number of the grid points  $N_0$  and grid spacing  $\Delta x_0$ , we shall consider a set of nested dyadic grids up to level  $L < \log_2 N_0$ ,

$$G^k = \{x_j^k, \quad j = 0, \dots, N_k\}, \quad 0 \leq k \leq L, \quad (16)$$

where  $x_j^k = j\Delta x_k$  with  $\Delta x_k = 2^k \Delta x_0$ ,  $N_k = 2^{-k} N_0$  and the cell averages of function  $u$  at  $x_j^k$ :

$$\bar{u}_j^k = \frac{1}{\Delta x_k} \int_{x_{j-1}^k}^{x_j^k} u(x) dx, \quad (17)$$

Let  $\tilde{u}_{2j-1}^k$  be the approximation to  $\bar{u}_{2j-1}^k$  by a unique polynomial of degree  $2s$  that interpolates  $\bar{u}_{j+l}^k$ ,  $|l| \leq s$  at  $x_{j+l}^k$ , where  $r = 2s + 1$  is the order of approximation .

The approximation error (or multi-resolution coefficients)  $d_j^k = \bar{u}_{2j-1}^{k-1} - \tilde{u}_{2j-1}^{k-1}$ , at the  $k$  level and the grid point  $x_j$ , has the property that if  $u(x)$  has  $(p - 1)$  continuous derivatives and a jump discontinuity at its  $p$  derivative ( $[\cdot]$  and  $(\cdot)$  denote the jump and the derivatives of the function respectively), then

$$d_j^k \approx \begin{cases} [u^{(p)}] \Delta x_k^p & p \leq r \\ u^{(r)} \Delta x_k^r & p > r \end{cases}. \quad (18)$$

The multi-resolution coefficient  $d_j^k$  measures how close the data at the finer grid  $\{x_j^{k-1}\}$  can be interpolated by the data at the coarser grid  $\{x_j^k\}$ . From (18) it follows that

$$|d_{2j}^{k-1}| \approx 2^{-\bar{p}} |d_j^k|, \quad \bar{p} = \min\{p, r\}, \quad (19)$$

which implies that away from discontinuities, the MR coefficients  $\{d_j^k\}$  diminish in size with the refinement of the grid at smooth parts of the solution; close to discontinuities, they remain the same size, independent of the order  $r = 2s + 1$  and level  $k$  of multi-resolution analysis. Since in this work, the first level ( $k = 1$ ) MR coefficients  $\{d_j^1\}$  are more than sufficient in detecting high gradients and shocks, we will drop the superscript 1 from the  $d_j^1$  unless noted otherwise. Examples of the performance of the high order multi-level multi-resolution analysis in detecting discontinuities in the solution of nonlinear system of hyperbolic PDE can be found in [14].

The computational overhead of the multi-resolution analysis, which comprises a dot product of a two vectors of length equal to the order of the MR analysis at each grid point in each dimension of a single flow quantity only once before the Runge-Kutta time stepping scheme, is negligible. It is equivalent to doing three more derivatives using CFD scheme in each Runge-Kutta step and its cost is insignificant when compared to the cost of finding a non-oscillatory representation of the derivative of the flux by the WENO scheme. The enhanced solution is well worth the minor additional CPU time.

## 2.4 Hybrid Scheme

Algorithmically, the Hybrid scheme is implemented with the following essential steps:

1. The multi-resolution analysis (MR) is performed in a given variable (usually density) only once at the beginning of the Runge-Kutta TVD time stepping scheme.

A grid point is flagged as non-smooth based on the smoothness sensor

$$\text{Flag}_i = \begin{cases} 1, & |d_i| > \epsilon_{MR} \\ 0, & \text{otherwise} \end{cases}, \quad (20)$$

where  $\epsilon_{MR}$  is a user tunable parameter.

2. A buffer zone is created around each grid point that is flagged as non-smooth.

If, for example, grid point,  $x_i$ , is flagged as non-smooth, then its  $m = \beta \frac{1}{2} \max(N_c, N_w + 1)$ , where  $\beta \geq 0$ ,  $N_c$  and  $N_w$  are the buffer zone factor, the order of CFD scheme and the order of WENO scheme, respectively, neighboring points  $\{x_{i-m}, \dots, x_i, \dots, x_{i+m}\}$  will also be designated as non-smooth, that is,  $\{\text{Flag}_j = 1, j = i - m, \dots, i, \dots, i + m\}$ . This condition prevents computation of the divergence of the Euler fluxes by the CFD scheme using non-smooth functional values.

3. The CFD scheme, which is computationally more efficient than WENO scheme, will compute the divergence of the flux over the full computational domain first. Then, the WENO scheme is employed to overwrite the divergence of the flux at those grid points designated as non-smooth by the flag.

**Remark 1** *Since the WENO coverage of the solution is USUALLY smaller than the CFD coverage, and since the CFD can be vectorized in a cache efficient manner along lines, it is logical to compute the redundant CFD solution that is going to be discarded and overwritten by the WENO later. Moreover, ease of programming and implementation should be considered. From experience, we know that the additional program complexity and additional labor cost is too high and the gain is too small to justify a more elaborat implementation. Of course, there are exceptions and those cases should be evaluated on a case by case basis. At the end of the day, it is the WALL clock time that should be improved.*

**Remark 2** *It is generally known that WENO is approximately five times more expensive than the corresponding CFD with similar order. According to the paper by Johnsen et al. [22], they estimated*

*the number of operations per grid point for CFD6, CFD8, WENO5 and WENO7 are 1100, 1600, 3100 and 6200 respectively, in computing the divergence of the convective fluxes. Since a WENO scheme is required to perform substantially more computations such as involved in the forming the eigensystem, flux splitting and forward and backward projections, five times more CPU time is a reasonable estimate. Of course, the actual efficiency of any implementation of the scheme is also highly depended on the competency of the programmer and data structures.*

**Remark 3** *The class of problems studied is restricted to those where the boundary conditions do not present any complications with the ghostpoints, for instance, periodic or freestream boundary conditions.*

*In this work, we shall use as many ghostpoints as required for a given order of the CFD scheme, the WENO scheme and the MR analysis. Also, the parameters  $\epsilon_{MR} = 1 \times 10^{-4}$  and  $\beta = 1$  are used typically.*

## 2.5 Numerical Results

The Hybrid scheme is tested on a three dimensional circular sonic jet injection in a Mach 2.1 supersonic cross flow with air according to the benchmark experiment performed by Schetz [32] and the computations performed later by Viti [33]. In the experiment a circular nozzle connects to a flat plate that is mounted parallel to the incoming supersonic flow. The flow field, as summarized in the schematic in figure 2, shows many flow features that are typical for sonic injection in supersonic cross stream. They include a laminar boundary layer that forms along the flat plate and a bow shock that forms ahead of the injector. The injected air at sonic speed expands rapidly into a plume and forms a barrel shock and a reflected shock. A contact slip line (shear layer) that

emanates from the injector edge is highly unstable and leads to the formation of small, unsteady vortex structures. The interaction between the bow shock and the boundary layer further leads to form a local separation of the laminar boundary layer underneath the bow shock.

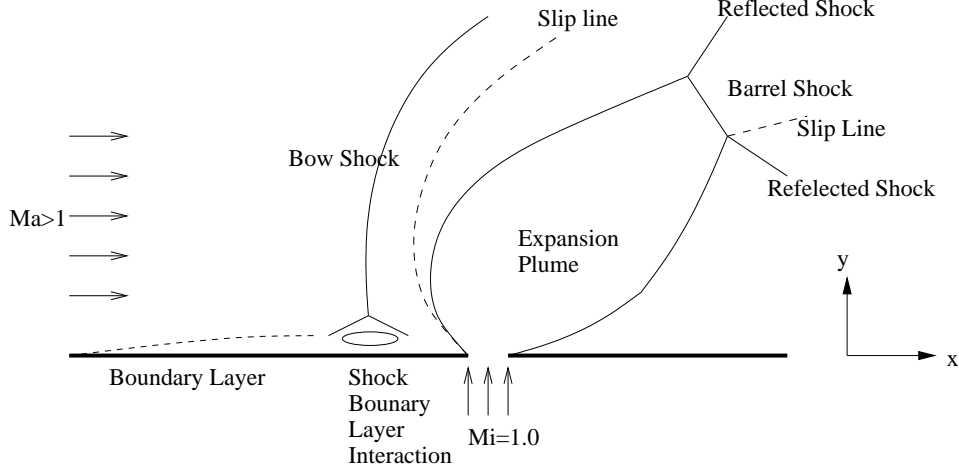


Figure 2: Schematic of flow features in a sonic injection in supersonic cross stream air flow.

Since the viscous effects are relatively small and since we are primarily interested in the performance of the Hybrid scheme in terms of accuracy and computational speed in this work, we compute the Schetz injector with the Hybrid *inviscid* Euler code. Since viscous effects are not accounted for, we are not able to capture the laminar boundary layer on the plate and the shock-boundary layer interaction. These viscous flow phenomena have only a minor influence on the large shock-expansion structures (bow shock, barrel shock, reflected shock, expansion plume and slip lines or shear layers). Moreover, with a high order Euler solver we are able to capture the more important small scale mixing structures in the unstable shear layers.

We consider a three dimensional rectangular domain with a supersonic cross-stream flow in  $x$ -direction and the sonic injection in  $z$ -direction. The rectangular computational domain size in  $x$ -,  $y$ - and  $z$ -direction is  $(4\text{cm} \times 1.5 \times 1\text{cm})$  with the origin located at  $(x_0, y_0, z_0) = (-2\text{cm}, 0\text{cm}, -0.5\text{cm})$ . The freestream Mach number, pressure and temperature are  $Ma_\infty = 2.1$ ,  $p_\infty = 11.1\text{kPa}$  and

$T_\infty = 159\text{K}$ , respectively. The injection Mach number, pressure and temperature are  $\text{Ma}_i = 1$ ,  $p_i = 364.8\text{kPa}$ , and  $T_i = 250\text{K}$ , respectively. The circular injector nozzle has a diameter of  $d_n = 0.389\text{cm}$  with the center located at  $(x_c, y_c, z_c) = (0\text{cm}, 0\text{cm}, 0\text{cm})$ . Computations were performed with non-dimensionalized variables based on a reference time scale of  $t_{ref} = 3.95 \times 10^{-5}\text{s}$ . The final non-dimensional time of  $T_f = 3$  time units or in dimensional units,  $T_f = 1.2 \times 10^{-4}\text{s}$ , is sufficiently long for the flow to reach a quasi-steady state in which most large scale structures are statistically invariant.

Free-stream conditions are specified at the  $x$  faces of the computational domain according to the supersonic cross-stream flow. In the  $y$ -direction, periodic boundary conditions are specified. On the bottom and top  $z$ -planes, a symmetry or zero mass flux condition is specified. The injector boundary condition is specified on ghost points (similar to the free stream conditions) and on grid points that are located within the circular injector region. The circular injector boundary geometry is hence approximated through a staircasing approximation in the Cartesian grid.

Three grid sizes as described in Table I were considered. The variables  $N_x, N_y$  and  $N_z$  denote the number of uniformly spaced grid points in the  $x$ -,  $y$ - and  $z$ -directions, respectively. Computations are performed with the Hybrid scheme, with approximation orders of  $2r - 1 = 3, 5$ , and  $7$  for WENO 4, 6, and 8 for CFD. We shall denote Hybrid-C $n$ W $m$ M $k$ G $i$  as an  $n$  order CFD scheme, a  $m$  order WENO-Z scheme and a  $k$  order MR analysis at a grid resolution case  $i$  in the following discussion. For example, Hybrid-C8W7M8G4 means the Hybrid scheme with an eighth order CFD scheme, a seventh order WENO-Z scheme and an eighth order MR analysis at a grid resolution  $(N_x, N_y, N_z) = (500, 167, 111)$ . In general, for a given  $M = 2r - 1$  order WENO-Z scheme, we will set  $n = k = m + 1$  in the computations performed in this study. An  $n + 2$  order smoothing of the solution in the smooth regions of the domain is performed at the end of a Runge-Kutta TVD time

stepping.

Grids	$N_x$	$N_y$	$N_z$
1	360	135	90
2	400	150	100
3	444	167	111
4	500	167	111

Table I: Grid sizes used in the computation of the jet interaction in a Mach 2.1 supersonic cross flow with air.

To avoid large and complicated three dimensional plots, that do not add significantly to the performance assessment of the Hybrid scheme, we focus on the visualization of flooded contour fields of relevant variables (mainly, density  $\rho$ , Mach number  $\text{Ma}$  and vorticity  $\omega$ ) with a two dimensional  $x - z$  plane cut at the center  $y = y^* = 0.75\text{cm}$  of the three dimensional physical domain.

The three dimensional simulations of this problem capture the evolution of the small scale eddies along the unstable slip line that plays an important role in the formation of transverse vortex tubes around the injecting jet. In figure 3, the temporal evolution of the density  $\rho(x, y^*, z, t_n)$  and Mach number  $\text{Ma}(x, y^*, z, t_n)$  are shown via a two dimensional  $x - z$  plane cut with  $y = y^* = 0.75\text{cm}$  as well as the three dimensional two levels iso-surfaces of the Mach number  $\text{Ma}$ , from early times  $t$  until the final time  $t = 3$ , as computed by the Hybrid-C8W7M8G4 scheme. The Hybrid scheme captures the long time evolution of the large scales structures (bow shock, barrel shock, reflected shock and expansion plume) as well as the small scales eddies structures (vortical rollups along the slip line) in an accurate and efficient manner as we will discuss in detail below. The instabilities

near the base of the injector jet lead to the formation of coherent structures between the bow shock and the expansion plume.

To justify the use of the high order (resolution) Hybrid scheme, we plot, in figure 4, the two dimensional density contour fields with increasing grid resolutions in the  $x$ -direction by 100 grid points and with increasing order of the WENO-Z scheme from the  $m = 2r - 1 = 3, 5$  and  $7$  with corresponding order of the CFD scheme and the MR analysis as discussed above. The low order and low grid resolution Hybrid scheme fails to capture the small scales eddies along the unstable slip lines but perform much better with increasing order and grid resolution. For low order scheme, the high numerical dissipation inherited in the underlying scheme requires a significant grid refinement to capture the small scales eddies. However, the increasing of grid resolution imposes a severe stress on the computational hardware in terms of memory and CPU time. It is recommended that high order scheme should be used whenever possible for accurate capturing of small scales structures in a long time flow evolution.

In figure 5, the density  $\rho$ , Mach number  $Ma$  and vorticity  $\omega$  contours are visualized at  $t=3$  as computed via a pure WENO-Z scheme and the Hybrid scheme with various orders with a fixed grid resolution  $(N_x, N_y, N_z) = (444, 167, 111)$ . The large scales structures in Hybrid and pure WENO computations are in good agreement except for minor differences in the small scales structures along the unstable slip lines between the bow shock and the expansion plume. The minor differences are a result of the slightly different level of dissipation in the WENO and CFD schemes at the same grid location and time. This translates in a slightly different flow behavior of the small scales structures even if they are evolved in time by the same time stepping scheme. Similar results and remarks are obtained with other grid resolutions (not shown).

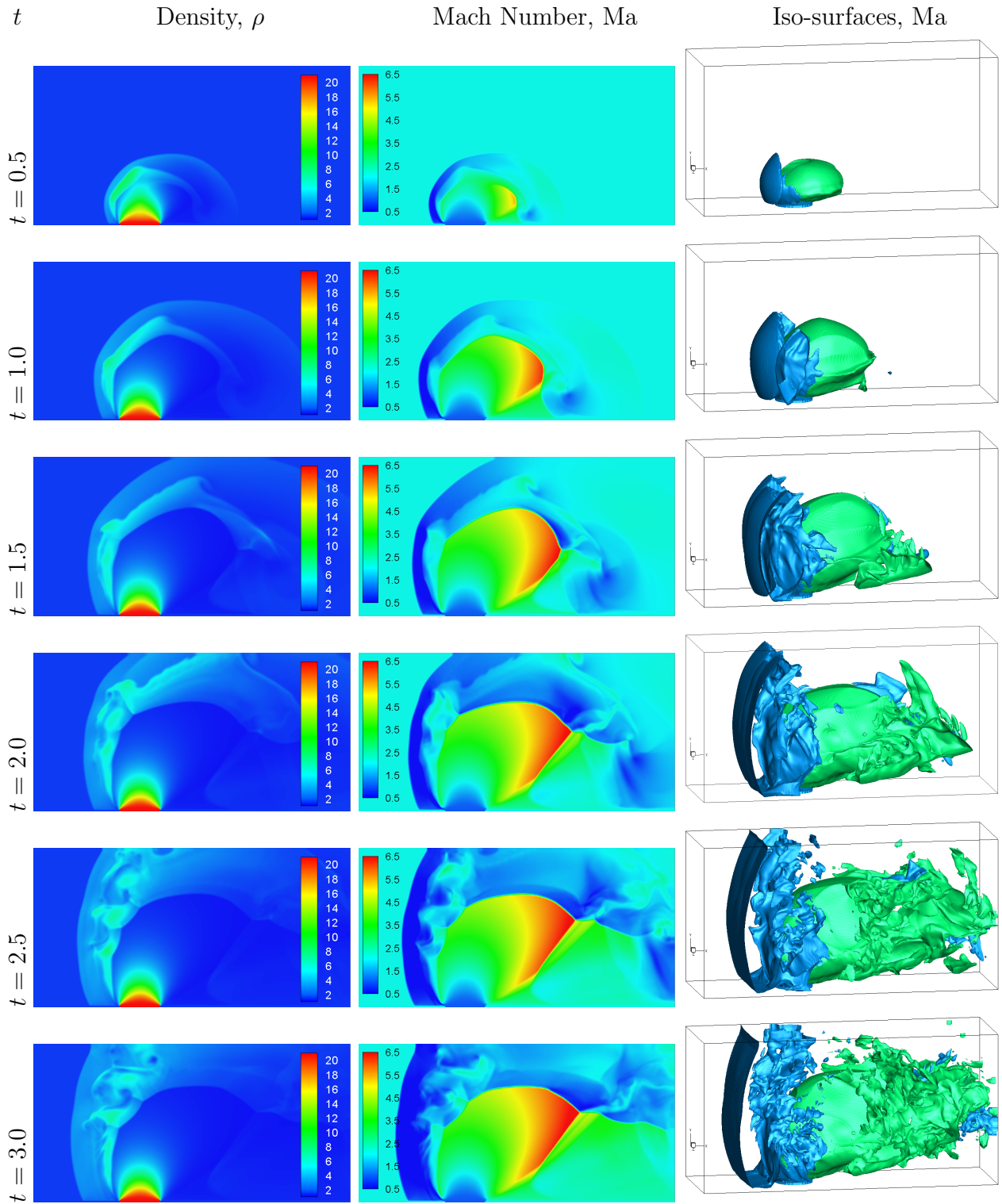


Figure 3: Temporal evolution of density  $\rho$  (left column) and Mach number  $Ma$  (middle column) at the center  $y^* = 0.75\text{cm}$  are shown at various times as computed by the Hybrid-C8W7M8G4 scheme. The iso-surfaces of the Mach number (right column) are also given.

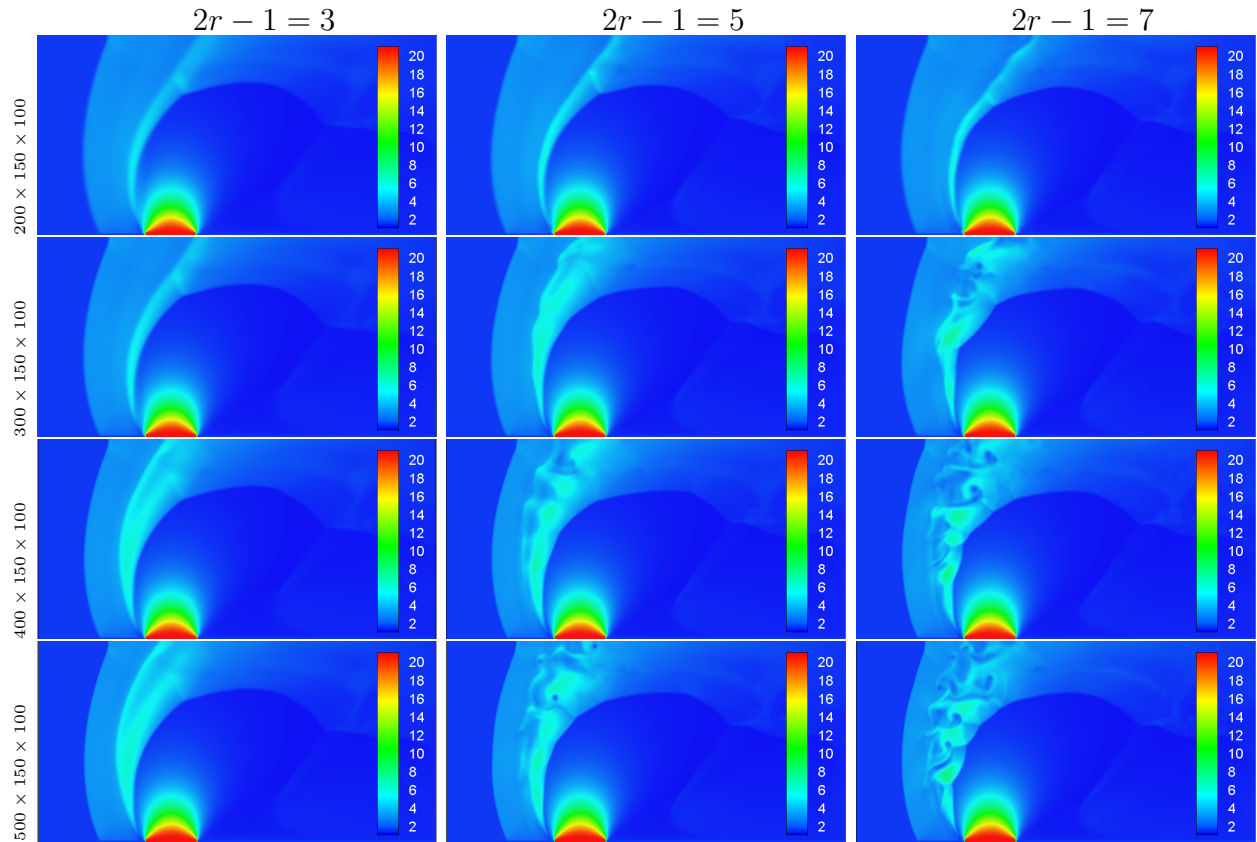


Figure 4: The two dimensional  $x - z$  plane cut of the density fields as computed by the Hybrid scheme with various orders and grid resolutions at time  $t = 3$ .

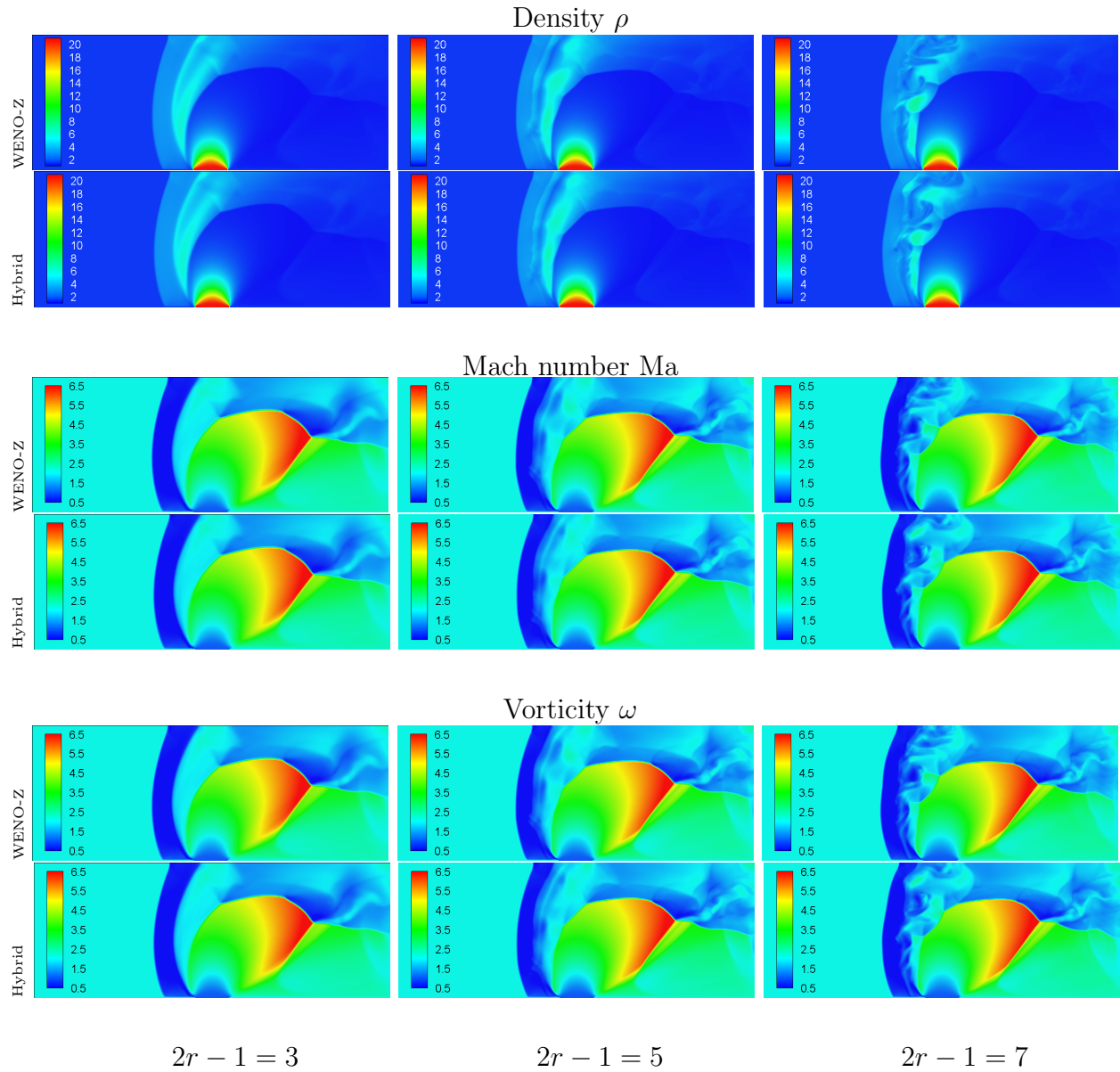


Figure 5: The two-dimensional  $x - z$  plane cut of density  $\rho$ , Mach number  $Ma$  and vorticity  $\omega$  as computed by a pure WENO-Z scheme and the Hybrid scheme with various orders at time  $t = 3$ . The grid resolution is  $(N_x, N_y, N_z) = (444, 167, 111)$ .

Computations were performed on an eight nodes cluster with 8 Intel Xeon cores per node at a clock speed of 2.5 GHz. All computations were run on eight cores. The computational domain with uniform grid spacing was partitioned using Cartesian domain decomposition. The parallel speed-up for this code and case up to eight processors is ideal. The CPU timing of the runs to time  $t = 3$  is shown in Table II.

Cases	$2r - 1 = 3$		$2r - 1 = 5$		$2r - 1 = 7$	
	WENO	Hybrid	WENO	Hybrid	WENO	Hybrid
$360 \times 135 \times 90$ (a)	2.8	2.2 (27%)	3.6	2.6 (38%)	4.5	3.1 (45%)
$400 \times 150 \times 100$ (b)	4.2	3.3 (27%)	5.4	3.7 (46%)	6.8	4.5 (51%)
$444 \times 167 \times 111$ (c)	6.5	4.9 (33%)	8.2	5.6 (46%)	10.3	6.6 (56%)

Table II: Timing in hours of the simulations at  $t = 3$  with a pure WENO-Z scheme and a Hybrid scheme of various orders and grid resolutions. The speedup in percentage is also given inside the parenthesis.

On average the Hybrid scheme is 40% faster than the pure WENO-Z scheme. The Hybrid scheme, on average, has a 35% coverage of WENO-Z scheme and hence a 65% coverage of the CFD scheme. With an increase of grid size from the small grid (a) to the large grid (c) in Table II, the percentage of WENO-Z coverage reduces as shown in the bar-plot in Figure 6. The reduced WENO-Z coverage lowers the normalized computational cost as shown versus the normalized grid size for different order  $2r - 1 = 3, 5$  and  $7$  in Fig. 6. At large orders,  $2r - 1$ , the reduction in WENO-Z coverage leads to a relatively larger increase in efficiency of the Hybrid as compared to the pure WENO-Z. At  $2r - 1 = 7$  and for the largest grid (c), the Hybrid improves the computational efficiency by 56%.

We note that with an increase in approximation order from  $2r - 1 = 3$  to  $7$ , the WENO-Z coverage

increases by approximately 10% (bar-plot in Figure 6). This means that the Hybrid scheme is relatively less efficient with increasing order because of the increased WENO coverage.

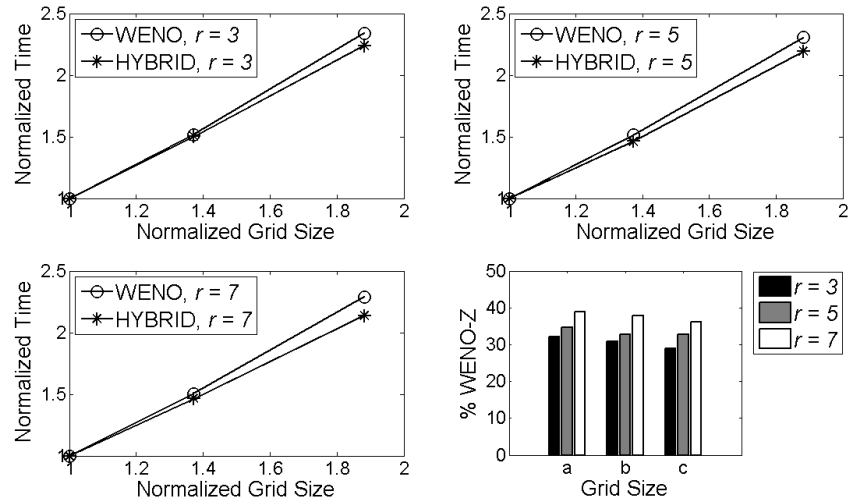


Figure 6: Comparison of timing results and percentage of WENO coverage used by the Hybrid scheme.

## 2.6 Conclusions

The high order Hybrid WENO-Z/Central finite difference Euler Solver is extended from two to three dimensions. The parallelized Hybrid scheme was tested on a sonic injector benchmark flow in supersonic cross stream. The Hybrid scheme uses the WENO-Z scheme in regions of the physical domain where the flow is not smooth and contains discontinuities such as contact discontinuities and shocks, whereas in smooth regions it uses a central finite difference scheme. The smoothness of the solution is quantified with a multi-resolution coefficient that is determined through a high order multi-resolution analysis on a single solution variable. Based on the multi-resolution coefficient, the Hybrid scheme switches dynamically between the computationally efficient central finite difference scheme and the computational more expensive WENO-Z scheme at each grid point and at each

time step.

The computational overhead of the multi-resolution analysis, which comprises a dot product of a two vectors of length equal to the order of the MR analysis at each grid point in each dimension of a single flow quantity before each Runge-Kutta time stepping scheme, is negligible as compared to the cost of finding a non-oscillatory representation of the derivative of the flux by the WENO scheme. The Hybrid scheme is hence more computationally efficient.

To illustrate the accuracy and efficiency, the Hybrid scheme was tested by means of computations of the benchmark flow problem of the sonic injection of fluid into a supersonic cross stream flow. The computations focused on a near injector flow region which features rich interaction between both large-scale shocks and expansions and the growth of small scale flow instabilities. In the initially uniform supersonic flow, the curved cross stream jet increasingly blocks the flow and as a result instabilities and shocks develop ahead and along of the curved cross-stream jet. Since the pressure of the jet is higher than the pressure in the cross stream, the jet expands and accelerates creating additional instabilities downstream, until it reaches a quasi-steady state.

For this flow computation 30% of the computational domain requires the use of WENO-Z scheme. With this a relatively large percentage of WENO-Z usage, the computation is up to 1.56 times faster with the Hybrid scheme than the one with a pure WENO-Z scheme. With increasing grid resolution, the WENO-Z coverage becomes relatively smaller, and the Hybrid scheme becomes relatively more efficient. For large computational domains, the lesser WENO-Z coverage is needed and hence computational cost should decrease further. On average the speed up with Hybrid scheme is 40% for the cases considered in this paper.

The flows computed with a Hybrid scheme and with a pure WENO-Z scheme are in very good

agreement. Hence, while the Hybrid scheme improves computational efficiency over the high order WENO-Z scheme, it does not reduce the accuracy. If anything, it is expected that the Hybrid scheme is more accurate, since the numerical dissipation and dispersion of the central difference schemes are smaller than WENO-Z scheme.

With an increasing order of underlying schemes, the capturing of the growth of small scale instabilities improves. With a third order scheme, the shear layer emanating from the injector jet is stable whereas at the fifth and seventh order scheme, the shear layer is unstable. Effectively, a lesser grid resolution is required with an increased order of approximation to obtain the same result. The lesser grid resolution reduces computational cost, which reduces the computational time by a factor that is dependent on the problem as well as choice of parameters of the numerical scheme. For the injector cases, with an increase of the order of approximation by two orders, similar results are obtained for grid resolution that require only half the computational time, i.e. another factor 2 of relative increase in computational efficiency.

### 3 Singular advection equation

We consider the numerical solution of the non-stationary singular advection equation:

$$\begin{cases} \frac{\partial u}{\partial t} + a \frac{\partial u}{\partial x} = \delta(x + ct), & x \in [-1, 1] \text{ and } t > 0, \\ u(x, 0) = \sin(\pi x), & x \in [-1, 1], \end{cases} \quad (21)$$

where  $a$  and  $c$  are non-zero fixed constants such that  $a + c \neq 0$ . With this restriction on  $a$  and  $c$ , we ensure that the analytical solution will have a local jump discontinuity at  $x = -ct$ .

The analytical solution for this problem is given by:

$$u(x, t) = \sin(\pi(x - at)) + \frac{1}{a + c}(H(x + ct) - H(x - at)),$$

where  $H$  is the Heaviside function defined as:

$$H(x) = \begin{cases} 0, & x < 0, \\ \frac{1}{2}, & x = 0, \\ 1 & x > 0. \end{cases}$$

### 3.1 Spectral Chebyshev collocation method

In this section we introduce the spectral methods and the discretization process, with particular emphasis in the Chebyshev collocation scheme with Gauss-Lobatto points.

In the solution of non-periodic problems, spectral methods are based in the following series expansion for the function  $u(x, t)$ :

$$u(x, t) = \sum_{k=0}^{\infty} \hat{u}_k(t) \phi_k(x),$$

where  $\{\phi_k(x)\}_{k \geq 0}$  are polynomials representing an orthogonal basis set for  $L_w[-1, 1]$ , the square integrable functions with respect to the weight function  $w(x)$  with the usual inner product in this space. The basis and weight functions are obtained as the solution of a specific Sturm-Liouville problem and the coefficients  $\hat{u}_k(t)$  are given by:

$$\hat{u}_k(t) = \frac{1}{\hat{\gamma}_k} \int_{-1}^1 u(x, t) \phi_k(x) w(x) dx, \quad \hat{\gamma}_k = \int_{-1}^1 \phi_k^2(x) w(x) dx.$$

The spectral approximation is obtained as a truncation of the previous series expansion, where a Gauss quadrature rule is used to replace the coefficients  $\hat{u}_k(t)$  for a suitable choice of points  $\{x_j\}_{j=0}^N$  and discrete weights  $\{w_j\}_{j=0}^N$ . If  $\tilde{u}_k(t)$  and  $\tilde{\gamma}_k$  denotes the respective approximations to  $\hat{u}_k(t)$  and

$\hat{\gamma}_k$  by the Gauss quadrature, then:

$$\tilde{u}_k(t) = \frac{1}{\tilde{\gamma}_k} \sum_{j=0}^N u(x_j, t) \phi_k(x_j) w_j, \quad \tilde{\gamma}_k = \sum_{j=0}^N \phi_k^2(x_j) w(x_j),$$

and the spectral approximation  $u^N(x, t)$  to  $u(x, t)$  is defined as:

$$\begin{aligned} u^N(x, t) &:= \sum_{k=0}^N \tilde{u}_k(t) \phi_k(x) \\ &= \sum_{k=0}^N \left( \frac{1}{\tilde{\gamma}_k} \sum_{j=0}^N u(x_j, t) \phi_k(x_j) w_j \right) \phi_k(x) \\ &= \sum_{j=0}^N u(x_j, t) \left( w_j \sum_{k=0}^N \frac{1}{\tilde{\gamma}_k} \phi_k(x_j) \phi_k(x) \right). \end{aligned}$$

In particular, the spectral Chebyshev method correspond to the choice of Chebyshev polynomials  $T_k(x) = \cos(k \arccos(x))$  as orthogonal basis set with respect to the weight function  $w(x) = (1 - x^2)^{-\frac{1}{2}}$ . In addition, we consider the Gauss-Lobatto points with discrete weights for the quadrature:

$$x_j = -\cos\left(\frac{\pi}{N}j\right), \quad w_j = \frac{\pi}{c_j N},$$

where  $c_0 = c_N = 2$  and  $c_j = 1$  for  $j = 1, 2, \dots, N - 1$ . The spectral Chebyshev approximation is expressed in terms of the Lagrange interpolation polynomial  $l_j(x)$  as follows:

$$u^N(x, t) = \sum_{j=0}^N u(x_j, t) l_j(x), \tag{22}$$

where  $l_j(x) = \frac{(-1)^{N+j+1}(1-x^2)}{c_j N^2(x-x_j)} \frac{dT_N}{dx}(x)$  is such that:

$$l_j(x_i) = \begin{cases} 1, & i = j, \\ 0, & i \neq j. \end{cases} \tag{23}$$

Additionally, the derivative  $\frac{\partial u}{\partial x}$  is approximated by differentiating (22). In particular, if the derivative is evaluated at the  $i^{\text{th}}$  quadrature node, for  $i = 0, 1, \dots, N$ , we obtain :

$$\frac{\partial u^N}{\partial x}(x_i, t) = \sum_{j=0}^N D_{ij} u(x_j, t), \tag{24}$$

where  $D_{ij} = \frac{dl_j}{dx} \Big|_{x=x_i}$  is a  $(N + 1) \times (N + 1)$  matrix representing the discrete spectral derivative operator, whose entries are:

$$D_{ij} = \begin{cases} -\frac{2N^2 + 1}{6}, & i = j = 0, \\ \frac{c_i (-1)^{i+j}}{c_j x_i - x_j}, & i \neq j, \\ -\frac{x_i}{2(1 - x_i^2)}, & i = j, \text{ for } i, j \in \{1, 2, \dots, N - 1\}, \\ \frac{2N^2 + 1}{6}, & i = j = N. \end{cases}$$

The collocation method consist in substitute the spectral Chebyshev approximation (22) in the advection equation (21) and evaluate the resulting expression at  $x = x_i$ , for each quadrature node  $x_i$ . Thus, we obtain the following system of ordinary differential equations (ODE):

$$\frac{du}{dt}(x_i, t) + a \sum_{j=0}^N D_{ij} u(x_j, t) = \delta(x_i + ct), \text{ for } i = 0, 1, \dots, N, \quad (25)$$

which can be integrated in time using the third order total variation diminishing (TVD) Runge-Kutta scheme. The respective numerical solution to this ODE will represent the approximate solution to (21) through the spectral Chebyshev collocation method with Gauss-Lobatto points.

### 3.2 The Dirac delta function

In the next section, we introduce some important properties of the  $\delta$ -function, useful to construct numerical approximations of it.

The  $\delta$ -function was introduced by Paul Dirac in order to create the mathematical tools for the development of quantum field theory, and currently, is with notable success used in applied mathematics and mathematical physics. Some properties of particular interest in this work are the following:

1.  $\int_{-\infty}^{\infty} \delta(x) dx = 1.$

2. Let  $(a, b) \subseteq \mathbb{R}$  a real interval and  $f(x)$  a continuous function in a neighborhood of  $x_0 \in (a, b)$ , then:

$$\int_a^b f(x)\delta(x - x_0) dx = f(x_0).$$

Moreover, if  $f(x)$  is a function with  $n$  continuous derivatives in a neighborhood of  $x_0 \in (a, b)$ :

$$\int_a^b f(x) \frac{d^n \delta}{dx^n}(x - x_0) dx = (-1)^n \frac{d^n f}{dx^n}(x_0),$$

where  $\frac{d^n \delta}{dx^n}$  is known as the generalized  $n^{\text{th}}$  derivative of  $\delta$ .

3. The generalized derivative of the Heaviside function is given by:

$$\delta(x) = \frac{dH}{dx}(x).$$

Many of the numerical approximations to the  $\delta$ -function, are based on the properties 1-3 listed above. We consider the direct projection (DP) method, the Gaussian (G) approximation (which were used in [7, 8] to solve (25)) and a regularization technique with high order polynomials (P method) presented in [9].

The DP method is based on property 3 and the  $\delta$ -function on the right hand side of (25) is approximate using the spectral derivative operator  $D_{ij}$  as:

$$\delta^{\text{DP}}(x_i + ct) = \sum_{j=0}^N D_{ij} H(x_j + ct).$$

The G approximation is defined as:

$$\delta_\varepsilon^{\text{G}}(x) = \frac{1}{2\sqrt{\pi\varepsilon}} \exp\left(-\frac{x^2}{4\varepsilon}\right),$$

which satisfy property 1 for all  $\varepsilon > 0$  and property 2 when  $\varepsilon$  tends to zero, that is:

$$\lim_{\varepsilon \rightarrow 0} \int_{-\infty}^{\infty} f(x)\delta_\varepsilon^{\text{G}}(x - x_0) dx = f(x_0).$$

We have developed a P method, where the  $\delta$ -function is approximated by:

$$\delta_\varepsilon^{P^{m,k}}(x) = \begin{cases} \frac{1}{\varepsilon} P^{m,k}\left(\frac{x}{\varepsilon}\right), & |x| \leq \varepsilon, \\ 0, & |x| > \varepsilon. \end{cases}$$

Here  $P^{m,k}(\xi)$ , for  $\xi \in [-1, 1]$ , is a polynomial of degree  $2\left(\left\lfloor \frac{m}{2} \right\rfloor + k + 1\right)$  containing only even powers of  $\xi$ , given by:

$$P^{m,k}(\xi) = c(1 - \xi^2)^{k+1}Q(\xi), \quad Q(\xi) = 1 - \sum_{j=1}^{\lfloor m/2 \rfloor} \langle 1, r_{2j} \rangle_k r_{2j}, \quad (26)$$

where  $\langle \cdot, \cdot \rangle_k$  is the usual inner product in  $L_{w_k}[-1, 1]$ ,  $w_k(\xi) = (1 - \xi^2)^{k+1}$ ,  $\{r_j\}_{j=1}^m$  is an orthonormal basis set for  $\text{span}\{1, \xi, \dots, \xi^m\}$  obtained with Gram-Schmidt orthogonalization procedure and  $c = \langle 1, Q \rangle_k$ . These polynomials satisfy the following properties:

$$\begin{aligned} \int_{-1}^1 P^{m,k}(\xi) d\xi &= 1, \\ \left. \frac{d^\beta P^{m,k}}{d\xi^\beta} \right|_{\xi=\pm 1} &= 0, \quad \beta = 0, \dots, k, \\ \int_{-1}^1 P^{m,k}(\xi) \xi^\alpha d\xi &= 0, \quad \alpha = 1, \dots, m. \end{aligned}$$

The first condition in (26) ensures that  $\delta_\varepsilon^{P^{m,k}}$  satisfy property 1 and the second one establishes the continuity of the derivatives up to order  $k$ . The third condition, known as moments condition, indicates that  $P^{m,k}$  has  $m$  vanishing moments and as a consequence of it, can be proven [9] that the accuracy in the approximation by  $\delta_\varepsilon^{P^{m,k}}(x)$ , in terms of property 2, is given by:

$$\int_{-\infty}^{\infty} f(x) \delta_\varepsilon^{P^{m,k}}(x - x_0) dx = f(x_0) + \mathcal{O}(\varepsilon^{m+1}),$$

for  $x_0 \in \mathbb{R}$  and  $f$  with at least  $m$  continuous derivatives.

Based on property 3, the approximation  $\delta_\varepsilon^{P^{m,k}}(x)$  induces a regularized approximation to the

Heaviside function with  $k + 1$  continuous derivatives, as follows:

$$\begin{aligned}
 H_\varepsilon^{m,k}(x) &= \int_{-\infty}^x \delta_\varepsilon^{P^{m,k}}(s) ds = \int_{-\varepsilon}^x \delta_\varepsilon^{P^{m,k}}(s) ds \\
 &= \begin{cases} 1, & x > \varepsilon, \\ R^{m,k}\left(\frac{x}{\varepsilon}\right), & |x| \leq \varepsilon, \\ 0, & x < -\varepsilon, \end{cases}
 \end{aligned}$$

where:

$$R^{m,k}(\xi) = \int_{-1}^{\xi} P^{m+1,k-1}(s) ds \quad \xi \in [-1, 1]. \quad (27)$$

As in the DP method, we will consider the following approximation to the  $\delta$ -function using the regularized Heaviside function:

$$\delta_\varepsilon^{\text{DP}^{m,k}}(x_i + ct) = \sum_{j=0}^N D_{ij} H_\varepsilon^{m,k}(x_j + ct).$$

In particular, we will use the polynomials  $P^{m=3,k=2}$  and  $R^{m=2,k=2}$  defined by (26) and (27) to approximate the  $\delta$ -function and Heaviside function:

$$\begin{aligned}
 P^{3,2}(\xi) &= \frac{315}{512}(3 - 20\xi^2 + 42\xi^4 - 36\xi^6 + 11\xi^8), \\
 R^{2,2}(\xi) &= \frac{1}{2} + \frac{1}{64}(105\xi - 175\xi^3 + 147\xi^5 - 45\xi^7).
 \end{aligned}$$

The next section describes the numerical experiments in the solution of the advection equation using the spectral Chebyshev collocation method with the approximations to the  $\delta$ -function described above.

### 3.3 Numerical experiments

This section presents numerical results in the implementation of the Chebyshev collocation method with Gauss-Lobatto points to compute an approximate solution of the advection equation (21)

for  $a = 1$  and  $c = \frac{1}{4}$  at  $t_{\max} = 2$ . To evaluate the  $\delta$ -function in (25), we will compare the approximations  $\delta^{\text{DP}}$ ,  $\delta_\varepsilon^{\text{G}}$ ,  $\delta_\varepsilon^{P^{3,2}}$  and  $\delta_\varepsilon^{\text{DP}^{2,2}}$ , described in section 3.2. For spatial discretization are considered  $N + 1 = 61, 121, 241$  collocation points and to solve to the ODE (25), a third order TVD Runge-Kutta scheme is used for time integration, with time step  $\Delta t = \frac{\lambda}{aN^2}$ , where  $\lambda = 0.5$  represent the Courant-Friedrichs-Lewy (CFL) number.

We present plots of analytical solution versus the spectral approximation (figure 8), logarithmic plots of the pointwise error (figure 9) and pointwise convergence order (figure 10 and table III), which are defined respectively as:

$$\begin{aligned} E(N, x_j, t_{\max}) &= |u(x_j, t_{\max}) - u^N(x_j, t_{\max})|, \\ q(N, x_j, t_{\max}) &= \log_2 \left| \frac{u^N(x_j, t_{\max}) - u^{2N}(x_j, t_{\max})}{u^{2N}(x_j, t_{\max}) - u^{4N}(x_j, t_{\max})} \right|, \end{aligned}$$

for each collocation point  $x_j$  in the coarser grid.

We first consider the  $\delta^{\text{DP}}$  and  $\delta_\varepsilon^{\text{G}}$ , which were used in [7, 8] for this problem and subsequently compare it with our P method.

The DP method leads to an inaccurate numerical solution, characterized by an oscillatory behavior, as figure 7 shows. In the  $\delta_\varepsilon^{\text{G}}$  approximation we considered  $\varepsilon = \frac{2}{N^2}$ , which is suggested in [7]. For this case, the numerical solution does not exhibit the oscillatory behavior and it yields a first order convergence in the jump discontinuity (figure 8-(a)). Despite the refinement of the grid, is not observed a significant difference in the reduction of the error, moreover, the numerical solution is not in the asymptotic range of convergence. Both results are consistent with [7, 8].

With respect to the approximations  $\delta_\varepsilon^{P^{3,2}}$  and  $\delta_\varepsilon^{\text{DP}^{2,2}}$ , we consider the heuristic choice  $\varepsilon = x_{\frac{N}{2}+3}$  on the coarser grid (that is, for  $N = 60$ ), which represent the second node to the right of zero. This

choice obeys to the fact that the convergence is first order in a neighborhood of the discontinuity and when  $\varepsilon$  increase, the accuracy of the numerical solution on  $[-\varepsilon, \varepsilon]$  will be impacted negatively. The numerical solution obtained with the P methods leads to a non-oscillatory solution (figures 8-(b) and 8-(c)). The convergence is first order in the discontinuity, but unlike the G method, away of the singularity the error decrease when the grid is refined and the solutions exhibit an asymptotic behavior at the formal order of the scheme (figures 9-(a), 9-(b) and 9-(c)), being approximately in accordance to figures 10-(a), 10-(b), 10-(c) and table III, first, fifth and fourth order accurate for  $\delta_\varepsilon^G$ ,  $\delta_\varepsilon^{P^{3,2}}$  and  $\delta_\varepsilon^{DP^{2,2}}$ , respectively.

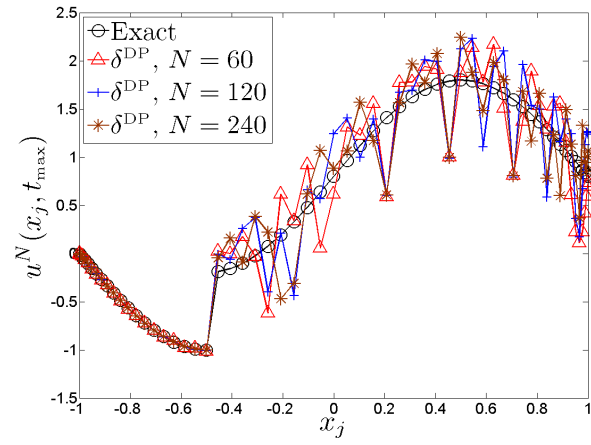


Figure 7: Exact versus numerical solution on the coarser grid, using  $\delta^{\text{DP}}$ , for  $N = 60, 120, 240$ .

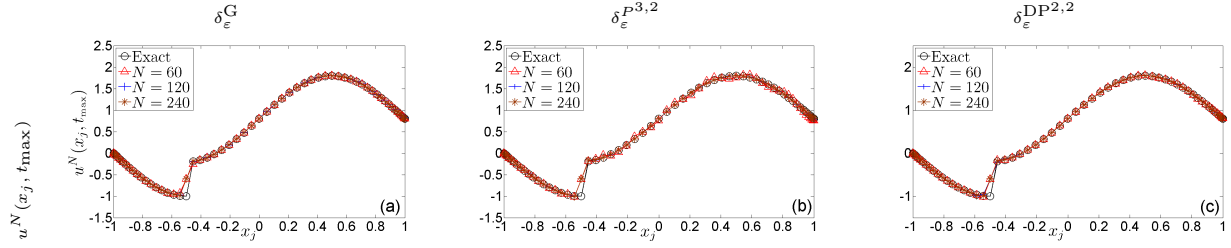


Figure 8: Exact versus numerical solution on the coarser grid, using  $\delta_\epsilon^G$  (a),  $\delta_\epsilon^{P^{3,2}}$  (b) and  $\delta_\epsilon^{DP^{2,2}}$  (c), for  $N = 60, 120, 240$ .

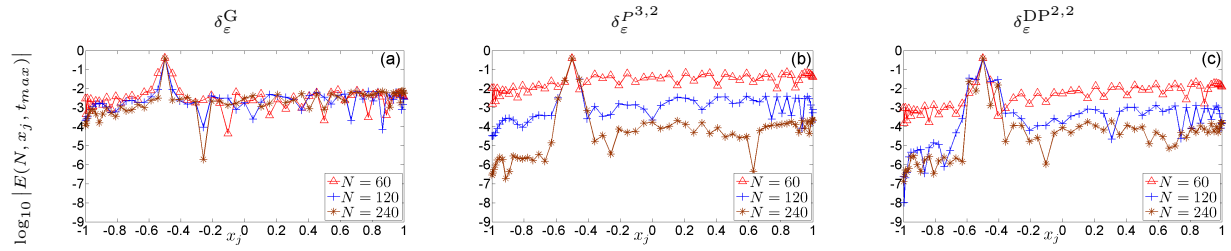


Figure 9:  $\log_{10}$  of the pointwise error on the coarser grid, using  $\delta_\epsilon^G$  (a),  $\delta_\epsilon^{P^{3,2}}$  (b) and  $\delta_\epsilon^{DP^{2,2}}$  (c), for  $N = 60, 120, 240$ .

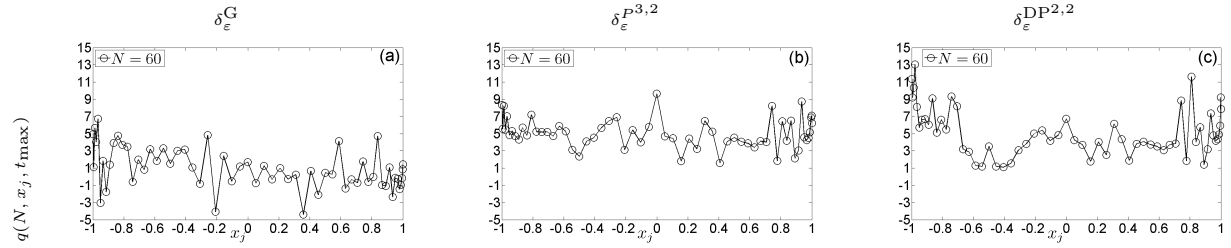


Figure 10: Pointwise convergence order on the coarser grid, using  $\delta_\epsilon^G$  (a),  $\delta_\epsilon^{P^{3,2}}$  (b) and  $\delta_\epsilon^{DP^{2,2}}$  (c), for  $N = 60$ .

$\bar{q}(N)$		
$\delta_\varepsilon^G$	$\delta_\varepsilon^{P^{3,2}}$	$\delta_\varepsilon^{\text{DP}^{2,2}}$
1.1	5.1	3.8

Table III: Averaged convergence order  $\bar{q}(N) = \frac{1}{N+1} \sum_{j=0}^N q(N, x_j, t_{\max})$  for  $N = 60$ .

### 3.4 Conclusions

We present the Chebyshev spectral collocation method to compute a numerical solution of the non-stationary singular advection equation (3), where the singular source term was approximated by the DP, G and P methods. In the DP method, the  $\delta$ -function is expressed as the derivative of the Heaviside function through the discrete spectral derivative operator, the G method use a Gaussian distribution and the P method employs regularization techniques based on high order polynomials. with compact support.

The DP methods leads to a inaccurate numerical approximation characterized by oscillatory behavior, whereas the solution with the Gaussian function is free oscillation but first order accurate.

The P method approximation to the  $\delta$ -function has proven to be very effective. With the high order polynomials and the regularized Heaviside function, the numerical solution is approximately fifth and fourth order accurate, respectively. Moreover, the results shows that with a smooth approximation to the Heaviside function, the amplitude in the oscillations arising when the DP method is used, will decrease.

In the near future, we plan to develop the multi-domain spectral-WENO method for two and three dimensional simulations of flow-particle interactions through the PSIC formulation (1), using as

weighing functions, the high order polynomials presented in the solution of the advection equation.

## **Acknowledgments**

We would like to acknowledge the funding support of this research by the RGC grant HKBU-200910 from Hong Kong University Grant Council (Dr. Don Wai Sun), an AFOSR-Young Investigator Grant (AFOSR-F9550-09-1-0097), the support by NSF (NSF-DMS-1115705) (Dr. Gustaaf Jacobs) and the CSRC at San Diego State University (Dr. Jose Castillo). We further extend our gratitude to Prof. Parra at the University of Valladolid for her efforts in the exchange program of students between the University of Valladolid and San Diego State University and the exchange student Antonio de Gregorio for their collaboration in this work.

## References

- [1] Wai-Sun Don and Antonio de Gregorio and Jean-Piero Suarez and Gustaaf B. Jacobs *Assesing the Performance of a Three Dimensional Hybrid Central/WENO Finite Difference Scheme with Computation of a Sonic Injector in Supersonic Cross Flow*, Submitted on March 2012 to the Journal: Advances in Applied Mathematics and Mechanics.
- [2] D. Kopriva, *Implementing Spectral Methods for Partial Differential Equations*, Springer-Verlag New York (2009)
- [3] C. K. Birsdall and A. B. Langdon, *Plasma Physics via Computer Simulation*, McGraw-Hill, Inc.(1985)
- [4] Chi-Wang Shu, *High Order Weighted Essentially Nonoscillatory Schemes for Convection Dominated Problems*, SIAM Rev, **51**, pp. 82-126 (2009)
- [5] P. L. ROE, *Proceedings, Seventh Int. Conf. Num. Meth. Fluid Dyn.*, Springer-Verlag, New York-Berlin, (1981)
- [6] Jacobs G. and Don W. S., *A high-order WENO-Z finite difference scheme based particle-source-incell method for computation of particle-laden flows with shocks*, J. Comput. Phys. **228**, pp. 1365–1379 (2008)
- [7] Jae-Hun Jung, *A Note on the Spectral Collocation Approximation of Some Differential Equations with Singular Source Terms*, J. Sci. Comput. **39**, pp. 1573–7691 (2008)
- [8] Jae-Hun Jung and Wai Sun Don, *Collocation Methods for Hyperbolic Partial Differential Equations with Singular Sources*, Adv. Appl. Math. Mech. **6**, pp. 769–780 (2009)

- [9] Anna-Karin Tornberg, *Multidimensional quadrature of singular and discontinuous functions*, BIT Numerical Mathematics **42**, pp. 644-669 (2002)
- [10] W. Rudin, *Functional Analysis*, McGraw-Hill, (1973)
- [11] C. W. Shu, *High order weighted essentially non-oscillatory schemes for convection dominated problems*, SIAM Rev. **51**, pp. 82–126 (2009)
- [12] A. Harten, *High resolution schemes for hyperbolic conservation laws*, J. Comput. Phys. **49**, pp. 357–393 (1983)
- [13] A. K. Henrick, T. D. Aslam and J. M. Powers, *Mapped weighted essentially non-oscillatory schemes: Achieving optimal order near critical points*, J. Comput. Phys. **207**, pp. 542–567 (2005)
- [14] B. Costa and W. S. Don, *High order Hybrid Central-WENO finite difference scheme for conservation laws*, J. Comput. Applied Math. **204** No. 2, pp. 209–218 (2007)
- [15] B. Costa and W. S. Don, *Multi-domain hybrid spectral-WENO methods for hyperbolic conservation laws*, J. Comput. Phys. **224** No. 2, pp. 970–991 (2007)
- [16] B. Costa, W. S. Don, D. Gottlieb and R. Sendersky, *Two-dimensional multi-domain hybrid spectral-WENO methods for conservation laws*, Comm. in Comput. Phys. **1** No. 3, pp. 548–574 (2006)
- [17] R. Borges, M. Carmona, B. Costa and W. S. Don, *An improved weighted essentially non-oscillatory scheme for hyperbolic conservation laws*, J. Comput. Phys. **227**, pp. 3101–3211 (2008)

- [18] M. Castro, B. Costa and W. S. Don, *High order weighted essentially non-oscillatory WENO-Z schemes for hyperbolic conservation laws*, J. Comput. Phys. **230**, pp. 1766–1792 (2011)
- [19] Z. Gao, Z. Li and W. S. Don, *High Order Weighted Essentially Non-Oscillation Schemes for One-Dimensional Detonation Wave Simulations*, J. Comput. Math. **29** No. 6, pp. 623–638 (2011)
- [20] Z. Gao, Z. Li and W. S. Don, *High Order Weighted Essentially Non-Oscillation Schemes for Two-Dimensional Detonation Wave Simulations*, J. Sci. Comput., DOI: 10.1007/s10915-011-9569-0 (2012)
- [21] M. Latini, O. Schilling and W. S. Don, *Effects of order of WENO flux reconstruction and spatial resolution on reshocked two-dimensional Richtmyer-Meshkov instability*, J. Comput. Phys. **221**, pp. 805–836 (2007)
- [22] E. Johnsen, J. Larsson, A. V. Bhagatwala, W. H. Cabot, P. Moin, B. J. Olson, P. S. Rawat, S. K. Shankar, B. Sjogreen, H. C. Yee, X. Zhong, S. K. Lele, *Assessment of high-resolution methods for numerical simulations of compressible turbulence with shock waves*, J. Comput. Phys. **229**, pp. 1213–1237 (2010)
- [23] B. Fornberg, *Calculation of Weights in Finite Difference Formulas*, SIAM Rev. **40** No. 3, pp. 685–691 (1998)
- [24] O. Vasilyev, T. Lund and P. Moin, *A General Class of Commutative Filters for LES in Complex Geometries*, J. Comput. Phys. **146** No. 1, pp. 82–104 (1998)
- [25] N. Adams and K. Shariff *High-resolution hybrid compact-ENO scheme for shock-turbulence interaction problems*, J. Comput. Phys. **127**, pp. 27–51 (1996)

- [26] D. Hill and D. Pullin, *Hybrid tuned center-difference-WENO method for large eddy simulations in the presence of strong shocks*, J. Comput. Phys. **194**, pp. 435–450 (2004)
- [27] S. Pirozzoli, *Conservative Hybrid Compact-WENO schemes for Shock-Turbulence Interaction*, J. Comput. Phys. **178** No. 1, pp. 81–117 (2002)
- [28] D. W. Zingg, *Comparison of High-Accuracy Finite Difference Methods for Linear Wave Propagation*, SIAM J. Sci. Comput. **22** No. 2, pp. 476–502 (2000)
- [29] C. Bogey and C. Bailly, *A family of low dispersive and low dissipative explicit schemes for flow and noise computations*, J. Comput. Phys. **194**, pp. 194–214 (2004)
- [30] A. Choen, S. M. Kaber, S. Muller and M. Postel, *Fully Adaptive Multiresolution Finite Volume Schemes for Conservation Laws*, Math. Comput. **72** No. 241, pp. 183–225 (2001)
- [31] B. Bihari and A. Harten, *Multiresolution schemes for the numerical solution of 2-D Conservation Laws*, SIAM J. Sci. Comput. **18** Vol. 2, pp. 315–354 (1997)
- [32] J. A. Schetz, P. F. Hawkins and H. Lehman, *Structure of highly under-expanded transverse jets in a supersonic stream*, AIAA J. **35** No. 5, pp. 882–884 (1976)
- [33] V. Viti, *Numerical analysis of the jet interaction flowfield with a main jet and an array of smaller jets*, Ph.D. dissertation, Virginia Tech, (2002).